Journal of Materials Chemistry C

Dual-Stimulus Bilayer Hydrogel Actuators with Rapid, Reversible, Bidirectional Bending Behaviors

Journal:	*Journal of Materials Chemistry C*
Manuscript ID	TC-ART-01-2019-000180.R1
Article Type:	Paper
Date Submitted by the Author:	26-Feb-2019
Complete List of Authors:	He, Xiaomin; Zhejiang University of Technology, College of chemical Eng. And materials Sci. Sun, Yan; Zhejiang University of Technology, College of chemical Eng. And materials Sci. Wu, Jiahui; Zhejiang University of Technology, College of chemical Eng. And materials Sci. Wang, Yang; Zhejiang University of Technology, College of chemical Eng. And materials Sci. Chen, Feng; Zhejiang University of Technology Fan, Ping; Zhejiang University of Technology, College of Material Science and Technology Zhong, Mingqiang; Zhejiang University of Technology Xiao, Shengwei; Taizhou University, College of Medicine and Chemical Engineering Zhang, Dong; University of Akron, Chemical and Biomolecular Engineering Yang, Jintao; Zhejiang University of Technology, College of chemical Eng. And materials Sci. Zheng, Jie; University of Akron, Chemical and Biomolecular Engineering

Dual-Stimulus Bilayer Hydrogel Actuators with Rapid, Reversible, Bidirectional Bending Behaviors

Xiaomin He[†], Yan Sun[†], Jiahui Wu[†], Yang Wang[†], Feng Chen[†], Ping Fan[†], Mingqiang Zhong[†], Shengwei Xiao[‡], Dong Zhang[¶], Jintao Yang*[†], and Jie Zheng*[¶]

[†] College of Materials Science& Engineering
Zhejiang University of Technology, Hangzhou 310014, China

[‡] School of Pharmaceutical and Chemical Engineering
Taizhou University, Jiaojiang 318000, China

[¶] Department of Chemical and Biomolecular Engineering
The University of Akron, Akron, Ohio 44325, USA

***Corresponding Author: (**J.Y.) yangjt@zjut.edu.cn; (J.Z.) zhengj@uakron.edu

Keywords: PolyNIPAM, GO, Hydrogel, Bilayer structure, Actuation

Figure of Content

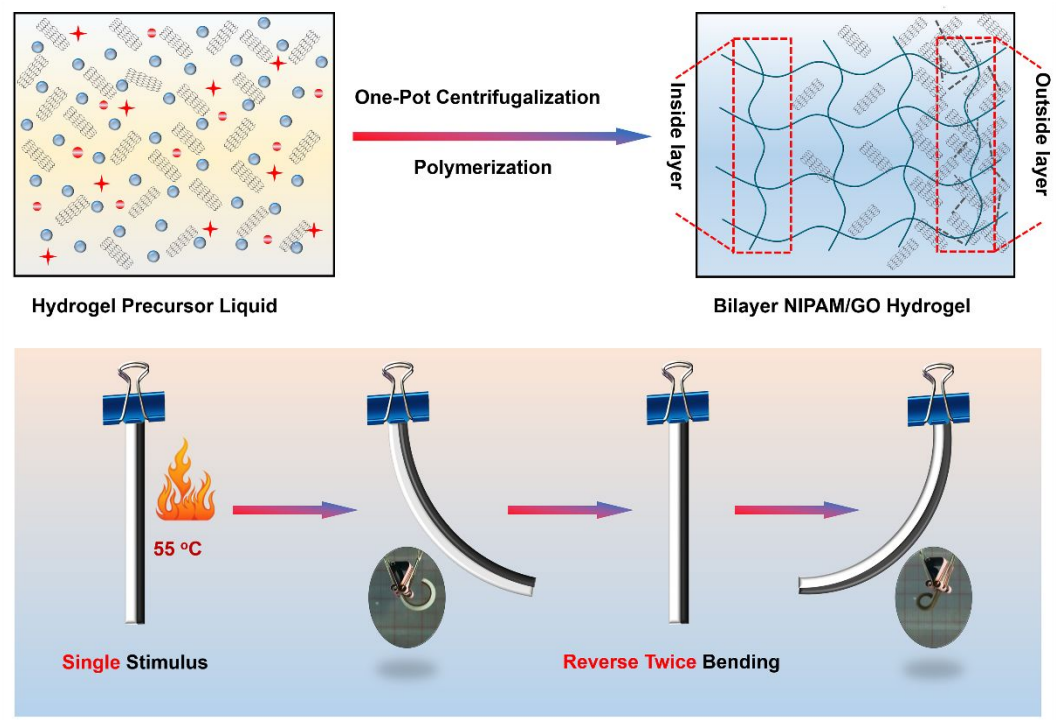

ABSTRACT

Developing new smart hydrogel systems and new fabrication methods is critical for fundamental research and industrial applications particularly in intelligent human-machine field, but still faces great challenges. In this work, we present bilayer poly(N-isopropylacrylamide)/graphene oxide (polyNIPAM/GO) hydrogels with dual thermo- and near-infrared (NIR)-responsive properties using a simple, in situ polymerization-centrifugation method. By tuning GO concentrations and centrifugation speeds, a transparent polyNIPAM layer and a dark-brown GO-rich layer are formed, where each layer displays distinct network structures and swelling behavior. Due to the asymmetric double-layer structure, the polyNIPAM/GO bilayer hydrogels enable to realize fast, controllable, bidirectional bending under thermal or NIR stimulation within 1 min., and bending orientation and degree can be reversibly, repeatedly, and precisely controlled by temperature- or NIR-induced cooperative swelling–shrinking properties from both layers. Based on the reversible, bi-directional bending nature of polyNIPAM/GO hydrogels, we further design two proof-of-concept hydrogel actuators to highlight the advantages of this hydrogel system: one acts as a wiggler to mimic robot arms to move objects, while the other serves as an electric switch to turn on/off a light. In addition, our polymerization-centrifugation method can also be used to prepare polyNIPAM/SiO_2 bilayer hydrogels, demonstrating its general applicability to other polyNIPAM–nanoparticle hydrogels with a bilayer structure. This work provides both new fabrication method and hybrid hydrogel systems for the development of smart, programmable, and versatile hydrogel-based actuators.

INTRODUCTION

Stimuli-responsive hydrogels have attracted a broad range of interests in fundamental research and practical applications, including artificial muscles, actuators, soft robotics, and human-machine interfaces.[1-11] Significant and continuous efforts have been made to develop stimuli-responsive hydrogels as smart and programmable materials, capable for changing their size, shape, conductivity, permeability, viscosity, mechanics, and other functional properties in response to different external stimuli (pH, temperature, light, force, ions, magnetic/electric field, and biochemical signals). [12-17] Different materials, nanofillers, and synthesis methods have been tested, separately or in combination, to develop a wide variety of stimuli-responsive hydrogels, such as thermos-responsive poly(N-isopropylacrylamide) (polyNIPAM), pH-responsive polyacrylic acid, and light-responsive graphene oxide(GO)-incorporated polyNIPAM composite hydrogels. Given the intrinsic swelling behaviors of hydrogels, shape morphing hydrogels are more commonly to be studied by selectively triggered site-specific swelling or contraction, leading to shape adaptability and transformation. However, the challenging still remains. Since the hydrogels are typically isotropic materials that usually undergo uniform volumetric expansion and contraction in response to stimuli, they are difficult to achieve asymmetrical shape changes such as bending, twisting, and folding.

To address this issue, the design of hybrid hydrogels with different (or even contrasting) components and network structures introduces a new strategy for stimuli-responsive smart hydrogels. Unlike single-layer hydrogels usually lacking of controllable shape transformation effect, bilayer hydrogels allow to integrate multiple, distinct or even opposite responses in two layers, each of which could be activated by particular stimuli.[2, 4, 9, 18-23] A general principle to design the shapeable bilayer hydrogels is to create a mismatch strain between the two layers by including different properties (e.g. softer vs. stiffer, swelling vs. non/less-swelling) in each layer. In this way, upon external stimulation, each layer undergoes volume expansion/contraction in certain positions or directions to different extents (i.e. the mismatch strain between the two layers), thus leading to macroscopic bending, stretching, and twisting. [5, 18, 20, 24-28] Different bilayer hydrogels in response to temperature, pH, salt, and light have been developed to realize the controllable shape changes for actuation, shape-memory, and self-healing applications.

Recently, nanoparticles (e.g. carbon nanotube, graphene, and clay)[17, 29-33] as crosslinkers and nanofillers have been often introduced into the hydrogels to construct a Janus bilayer or multilayer hydrogels through chemical or physical interactions (covalent bonds, hydrogen bonds, van der Waals) to adhere the two adjacent layers. [29-30] The resulting bilayer hydrogels not only improved their mechanical properties, but also possessed actuation capacity. Layer-by-layer method is commonly used to fabricate bilayer hydrogels. Kim et al[34] prepared a light-responsive bilayer hydrogel consisting of a polyNIPAM/rGO composite hydrogel as an active layer and a poly(acrylamide) hydrogel as a passive layer. Upon light irradiation, the volume of the active layer decreased, while the passive layer retained its original dimension, so that mismatch volume size induced the bending of the bilayer. Chu et al[35] prepared a thermo-responsive polyNIPAM/clay bilayer hydrogel, in which the two layers included different content of clay. The difference in thermo-responsive swelling/shrinking behavior between the two layers led to directional bending upon alternate heating and cooling. Similarly, Chen

et al[30] and Wang et al[36] fabricated (Na-alginate/polyNIPAM)/(Al-alginate/polyNIPAM) and (polyNIPAM)-clay/(polyNIPAM)-clay-GO hydrogels, respectively, and both hydrogels enable thermo-responsive and reversible actuation. While these nanocomposite hydrogels have hybrid and inhomogeneous structure, but the layer-by-layer fabrication processes are inconvenient or difficult to precisely achieve the gradient distributions of nanocomposites inside polymer networks.[38-45]

Another strategy has been proposed to use external fields (gravity, magnetic, or electric field) for constructing asymmetrical and gradient distribution of nanoparticles inside hydrogels in order to realize shapeable actuation.[33, 38, 40, 43, 45]The external fields will aid the directional migration and distribution of nanoparticles so as to ultimately achieve the concentration gradient of nanoparticles across the thickness of the hydrogel. [33, 38, 42-43] Such gradient distribution of nanoparticles in bilayer hydrogel network will cause asymmetric internal stress that would induce shape changes.[43] Among different shape changes, while bending actuation appears to be a the most simple deformation, bi-directional bending of hydrogels requires a delicate design and balance of driving forces in both hydrogel layers. In most cases, the bending of hydrogels in one direction is relatively simple, while bi-directional bending of hydrogels is only achievable under different environments or stimuli.[45] For instance, Jiang et al.[9] and Yang et al.[37] prepared bilayer hydrogels, which bent to one direction in aqueous solutions, but to an opposite direction in organic solvents, due to the cooperative asymmetric swelling/shrinking of the hydrogel and organogel networks. For both hydrogels, different external stimuli are required to achieve bi-directional bending. So, the remaining challenge is to develop a bilayer hydrogel capable of bending in different directions under a single external stimulus, which will greatly expand hydrogel-based actuator applications.

In this work, we developed a hybrid polyNIPAM/GO bilayer hydrogel, capable of achieving tunable, fast, and bidirectional bending under thermal or near-infrared radiation (NIR) stimulus. Upon polymerization, a high-gravity field was applied to drive GO sheets moving from one side of the hydrogel to another side, which generate a gradient distribution of GO sheets along the hydrogel thickness direction, thus forming a bilayer structure. The thickness of each layer can be readily tuned by centrifugation speed and GO content. Considering that GO films or laminates alone are too brittle to be bent, the integration of rigid GO into highly expandable polyNIPAM network via intermolecular interactions of hydrogen bonding, van der Waals force, and physical entanglement is expected to introduce controllable actuation behaviors. Under specific GO content and centrifugation speed, the resultant polyNIPAM/GO bilayer hydrogels enabled to bend toward the GO-rich layer in water due to the lower swelling ratio of this layer. At higher temperatures, the competition of different volume shrinkages between the GO-rich layer and the polyNIPAM layer would induce an opposite bending toward the polyNIPAM layer. As a result, the hydrogels showed fast, reversible, bi-directional bending actuation in response to thermal stimulus. Also, polyNIPAM/GO bilayer hydrogel showed similar NIR-triggered bending behavior. Furthermore, we designed two different temperature-responsive hydrogel actuators, which act as an electrical switch to turn on/off light and a wiggler to move an object. Overall, this bilayer hydrogel with reversible and programmable bending actuations expands the construction and application of smart soft-materials.

MATERIALS AND METHODS

Materials. N-Isopropylacrylamide (NIPAM, 97.0 %) was purchased from Sigma-Aldrich and

purified by recrystallization from hexanes. Graphene oxide (GO) with particle size in the range of 0.2 to 10 μm was purchased from Scott chemistry company. Potassium persulphate (KPS), N, N'-methylene-bisacrylamide (MBAA), and N, N, N', N'-tetramethylethylenediamine (TEMED) were purchased from Shanghai Aladdin Chemical Agent Co., Ltd. (China) com, and used as received.

Preparation of Bilayer PolyNIPAM/GO Composite Hydrogels. PolyNIPAM/GO composite hydrogels were prepared by one-pot method based on centrifugal force. Typically, GO aqueous suspension with specific concentration was prepared by magnetic stirring and followed ultrasonicating, subsequently, pre-specified amount of N-isopropyl-acrylamide (NIPAM) monomers was dissolved in the suspension. The resultant mixture was further vigorously stirred for 5 min, followed by the addition of pre-specified amounts of potassium persulfate (KPS), N, N'-methylene-bisacrylamide (MBAA) and N, N, N', N'-tetramethyl-ethylenediamine (TEMED). The reaction solution was quickly injected into a sealed mold with dimension of 30 × 10 × 1 mm (length, width, thickness). The mold was perpendicularly placed in the high speed centrifugal machine, and the reaction was carried out under specific centrifugation speed for 30 min. After the reaction, the prepared hydrogel was taken out and stored in deionized water. To distinguish the hydrogels, the hydrogel was named as GOn.Rm where GO and R are the abbreviations of graphene oxide and centrifugation speed, n and m represent the concentration of GO in the reaction solution, and centrifugation speed, respectively. As an example, GO1.R1000 hydrogel was the hydrogel prepared from GO suspension of 1.0 mg/ml and under centrifugation of 1000 rpm. In this study, for centrifugation speeds (e.g. 1000, 2000, 3000, 4000 rpm) were applied. According to the calculation of relative centrifugal force, shown as formula 1), the calculated relative centrifugal force were ~60, ~225, ~500, and 890 g, respectively.

$$RCF=1.18 \times 10^{-5} \times N^2 \times R \qquad 1)$$

RCF: Relative centrifugal force (g); N: Centrifuge speed (r/min); R: Centrifuge radius (cm).

Characterization of Bilayer PolyNIPAM/GO Composite Hydrogels. The hydrogels were freeze-dried for the characterization of chemical composition, structure and morphology. The composition of each layer of the bilayer sample was characterized by Raman spectroscopy (Renishaw Invia Plus) with resolution at 1.0 cm^{-1}. The morphology of the hydrogel was characterized by observing the fracture section of the freeze-dried hydrogel using SEM (FEI Nova Nano 450). The mechanical properties of the hydrogel were measured by a tensile tester (Instron MOD EL5567, MA) with a 100 N load 170 cell and a 100 mm min^{-1} of crosshead speed at room temperature. The tensile test specimen of the hydrogel was cut into a dumbbell-shaped (ASTM-638-V) with 16 mm gauge length, 4 mm width, and 1.0 mm thickness. The hydrogel was fixed in the fixture and stretched to break at 10 mm/min of strain rate. The tensile stress (σ) was calculated as $\sigma=F/A_0$, where F is the load and A_0 is the cross-sectional area of the original specimen. The tensile strain (ε) was defined as the elongation ($\triangle l$) relative to the initial length (l_0), $\varepsilon=\triangle l/ l_0 \times 100\%$.

RESULTS AND DISCUSSION

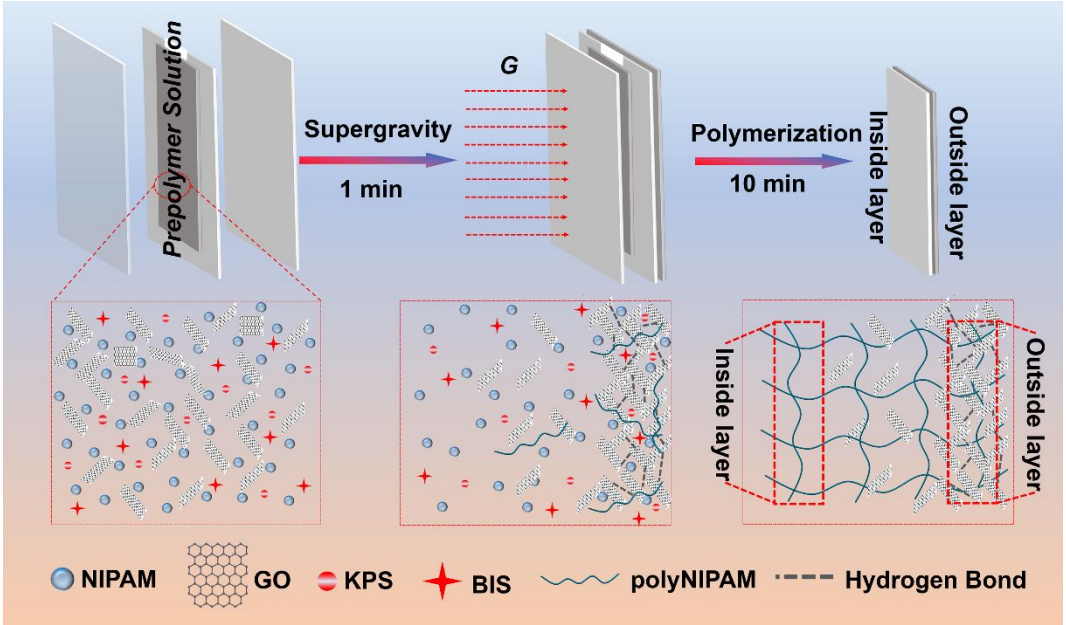

Figure 1. Schematic illustration of the fabrication process using in situ polymerization-centrifugation method.

Figure 1 shows the fabrication process of a polyNIPAM/GO bilayer hydrogel. Briefly, the precursor solution containing 1 mol/L NIPAM, 3.69 mmol/L KPS, 1.95 mmol/L MBAA, 6.67 mmol/L TEMED, and pre-specified concentration of GO was well mixed by vigorously stirring and ultrasonication, and then injected into a sealed mold. The reaction was carried out at ambient temperature and under a high-gravity field. Upon applying centrifugation during the polymerization, GO particles were moved from one side of hydrogel to another side due to a significant difference in density between GO particles and polyNIPAM, resulting in a bilayer structure. Using this method, we prepared four different polyNIPAM/GO hydrogels under different GO concentrations (1.0-3.0 mg/mL) and centrifugation speeds (1000-4000 rpm), i.e. (i) GO3.R1000 (GO concentration of 3 mg/ml and centrifugation speed of 1000 rpm), (ii) GO3.R4000, (iii) GO1.R1000, and (iv) GO1.R4000. At the first glance in **Figure 2a**, all of four as-prepared polyNIPAM/GO hydrogels displayed visible bilayer structure: a transparent polyNIPAM layer and a dark-brown GO-rich layer. The thickness of the two layers showed a strong dependence of GO concentration and centrifugation speed. GO1.R1000 and GO1.R4000 bilayer hydrogels prepared at a low GO concentration of 1.0 mg/ml showed much thinner dark-brown layer than GO3.R1000 and GO3.R4000 hydrogels prepared at a high GO concentration of 3.0 mg/ml. Meanwhile, at a given GO concentration (1.0 mg/mL), increases of centrifuge speed from 1000 to 4000 rpm led to not only an increase of the thickness ratio (i.e. dark-brown layer : transparent layer) of the two layers from 0.085 : 1 to 0.21 : 1, but also a much more distinct bilayer structure. So, the high centrifugation speed not only induced different layer thickness, but also affected the stacking of GO nanoparticles. The cross-sectional morphologies of different bilayer hydrogels were further characterized by SEM images. As shown in **Figure 2b**, all four hydrogels displayed a bilayer structure with distinct porous structures, where the transparent polyNIPAM layer showed a large porous structure with average pore sizes of ~58.1–86.9 μm, while the dark-brown GO-rich layer displayed a high density of smaller pores of ~41.9–54.9 μm. The difference in the pore sizes of both layers is a

result of GO physically crosslinking with polyNIPAM chains to form a more compact network. Such GO-enhanced physical crosslinking effect became more pronounced in the cases of GO1.R4000and GO3.R4000 samples. Hydrophilic hydroxyl and carboxyl groups from highly stacked GO not only enhance the interfacial interactions (hydrogel bond and van der Waals force, and physical entanglement) between the GO nanosheets and polyNIPAM chains, but also build a distinct physically crosslinked network in another layer. The intercalation of GO nanosheets in bilayer hydrogels was demonstrated by Raman spectra. In **Figure 2c**, Raman analysis of the two layers of the polyNIPAM/GO hydrogels showed that the dark-brown GO-rich layer exhibited exhibits two characteristic peaks of GO at 1345 cm^{-1} (D) and 1578 cm^{-1} (G), corresponding to the vibrations of sp3 carbon atoms with defects and the vibration of sp2 carbon atoms in a graphitic 2D hexagonal lattice, respectively. However, these two peaks were hardly observed in the transparent polyNIPAM layer. So, the results from Optical and Raman analysis confirm that GO has been successfully incorporated into the polyNIPAM hydrogel. As compared to other external fields (e.g. electric or magnetic field), the centrifugation-induced gravity exerts a much higher driving force to distribute GO particles into hydrogel network, leading to a bilayer structure.

As a demonstration, **Figure 2d** shows the typical tensile stress–strain curves of polyNIPAM/GO bilayer hydrogel and polyNIPAM single-layer hydrogel. It can be seen that pristine polyNIPAM displayed a tensile strength of ~27 kPa at a fracture stain of ~ 390 %. When incorporated with GO, bilayer hydrogels showed increased tensile strength of ~66 kPa at fracture strain of 394 % for GO1.R1000 and further increased tensile strength of ~83 kPa at fracture strain of 484 % for GO3.R1000, indicating that that the incorporation of GO into polyNIPAM hydrogel can greatly improve the mechanical properties. In addition, the centrifugation speed showed some effect on the mechanical properties of the hydrogel. The tensile stress-strain curves of the hydrogels prepared under different centrifugation speeds shown in **Figure S1** indicated that the distinct bilayer structure induced the slightly decrease in tensile properties. As an example, GO3.R1000 showed a tensile strength of ~83 kPa at a fracture strain of 484 %, while when the centrifugation speed was increased to 4000, the resultant GO3.R4000 hydrogel showed a lower tensile strength of ~49 kPa and a fracture strain of 496 %. The decreased tensile properties is likely because more GO sheets immigrated into one side of the hydrogel. However, in all cases, the polyNIPAM/GO bilayer hydrogel exhibits much stronger tensile properties than polyNIPAM single-layer hydrogel.

To better understand energy dissipation during the fracture process of polyNIPAM/GO bilayer hydrogels, we conducted the cyclic loading-unloading tests on GO1.R1000 and GO3.R3000 hydrogels prepared at different GO concentrations (1.0 mg/mL and 3.0 mg/mL) and different centrifuging speeds (1000 and 3000 rpm.). As shown in **Figure S2**, both GO1.R1000 and GO3.R3000 hydrogels experienced similar energy dissipation mode, i.e. hysteresis loops significantly increased with tensile strains. These results suggest that polyNIPAM/GO bilayer hydrogels possess obviously GO concentration-dependent and strain-dependent energy dissipation behaviors, and effective energy dissipation occurs at the higher GO concentrations and the higher strains. Meanwhile, as GO concentrations increased from 1.0 mg/ml to 3.0 mg/mL, the loop area became larger and dissipated more energy. While both hydrogels possessed low mechanical properties, the increase of GO concentrations can indeed increase the intermolecular interactions between polymer chains and GO nanosheets, leading to the larger hysteresis loop and the better energy dissipation.

Furthermore, we also carried out five successive loading-unloading cycles on the same GO1.R1000 and GO3.R3000 hydrogel samples at a constant strain of 300 % to test the self-recovery ability of the bilayer hydrogel (**Figure S3**). No resting time was applied to the hydrogels between any two consecutive loading cycles. Consistently, both hydrogels displayed the largest hysteresis loop area in the first loading-unloading cycle, but the immediate second cycle led to a significant reduction in hysteresis loops, which were retained almost unchanged in the 3rd-5th cycles. This indicates that after the first loading-unloading cycle, the hydrogel network is severely damaged and can not be recovered immediately, demonstrating the poor self-recovery property.

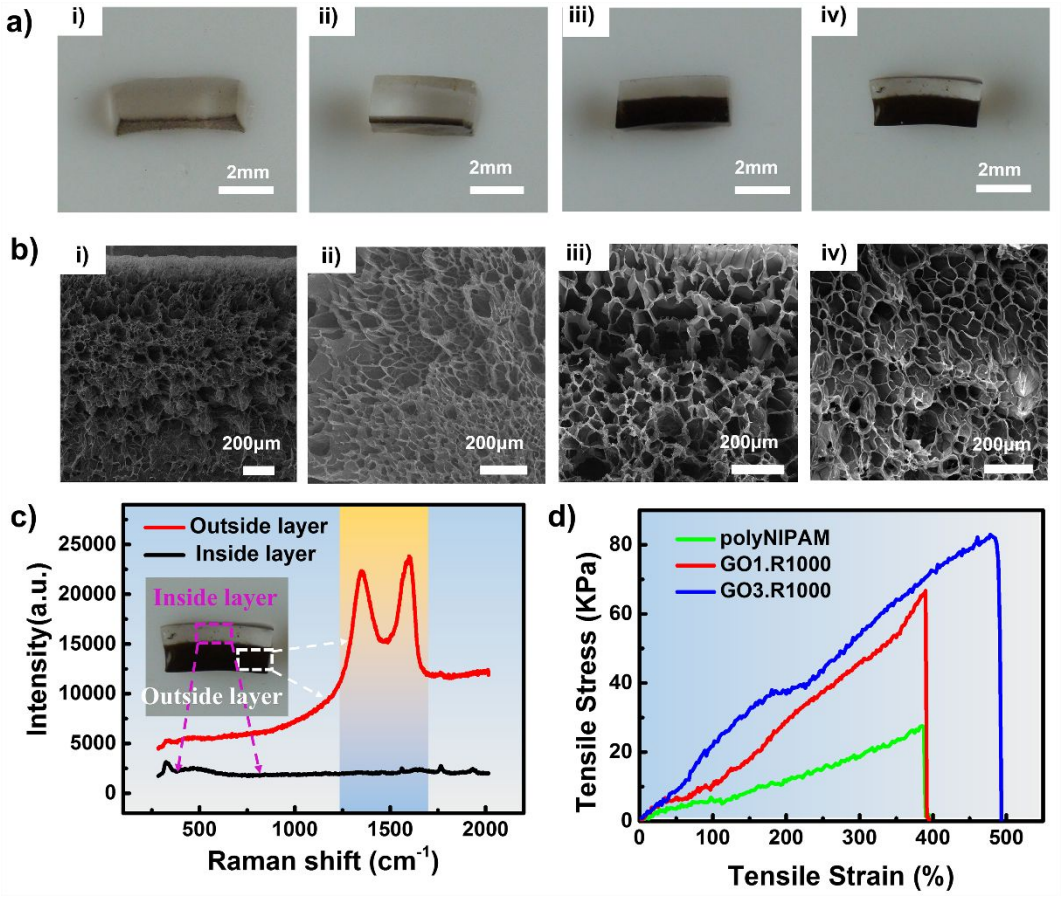

Figure 2. (a) Digital and (b) SEM images of (i) GO1.R1000, (ii) GO1.R4000, (iii) GO3.R1000, and (iv) GO3.R4000 bilayer hydrogels fabricated at different GO concentrations and centrifugation speeds. (c) Raman spectra of the two layers in GO3.R4000 bilayer hydrogel. (d) Tensile stress-strain curves of polyNIPAM hydrogel and polyNIPAM/GO bilayer hydrogel with different GO concentrations.

From a structural design viewpoint, the presence of a bilayer structure with contrasting swelling behaviors of the materials (i.e. non-swelling nature of GO and thermo-induced swelling of polyNIPAM) would induce different degrees of swelling/shrinkage characteristics for both layers, so that asymmetric stress would drives the hydrogel to bend in a different but controlled way. To better quantify the bending behavior of a hydrogel, **Figure 3a** shows a definition of a bending angle that is determined between a vertical vector and a vector connecting the original point and the end edge of

the hydrogel. Accordingly, a negative bending angle is defined as the bilayer hydrogel bends toward the GO-rich layer, while a positive bending angle is vice versa. First, bending kinetic of GO1.R1000, GO1.R2000, GO1.R3000, and GO1.R4000 hydrogels (GO concentration of 1.0 mg/mL and centrifugation speed of 1000, 2000, 3000, and 4000 rpm) in response to temperature change of water from 25 °C to 55 °C was measured, as shown in **Figure 3b**. Overall, when transferring all polyNIPAM/GO hydrogels from 25 °C water to 55 °C water, all hydrogels experienced a rapid increase of negative bending angle within 16-24 seconds. Specifically, a total change of bending angle was -192.2 ° for GO1.R1000, -199.9 ° for GO1.R2000, -220.3 ° for GO1.R3000, and -221.7 ° for GO1.R4000, respectively. It appeared that the hydrogels prepared at high centrifugation speeds (3000-4000 rpm) displayed the larger bending angle than those prepared at low centrifugation speeds (1000-2000 rpm), probably because high centrifugation speeds lead to a more distinct bilayer structure and thus a more contrasting swelling behaviors in both layers. It should be noted that due to the low thickness portion (max. ratio is ~20 % to the total thickness, as shown in Figure 2a) of the GO-rich layer when the GO concentration was 1.0 mg/mL, all bilayer hydrogels could only bend toward one direction (**Figure 3b** & **3d**).

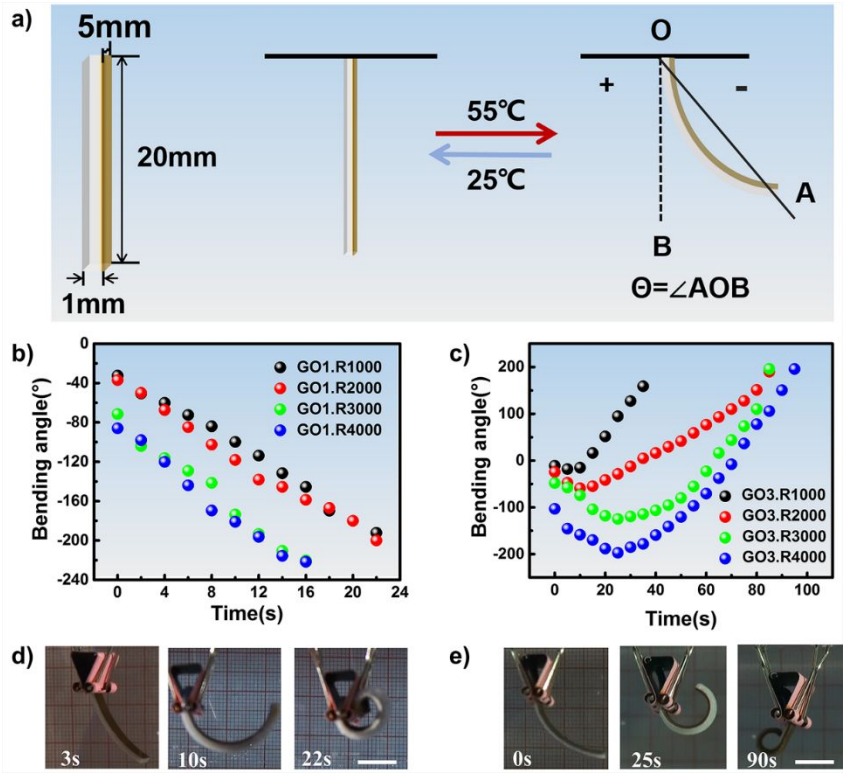

Figure 3. (a) Schematic bending of polyNIPAM/GO bilayer hydrogel and definition of the bending angle as Θ=∠AOB. Bending kinetics of polyNIPAM/GO bilayer hydrogels prepared at GO concentration of (b) 1.0 mg/ml and (c) 3.0 mg/ml and under different centrifugation speeds of 1000, 2000, 3000, and 4000 rpm. Typical images of (d) GO1.R1000 and (e) GO3.R3000 hydrogels during the bending process (scale bar=1 cm).

To overcome this single-direction bending limit, we prepared another group of polyNIPAM/GO hydrogels containing the higher GO concentration of 3.0 mg/ml. In **Figure 3c**, time-dependent thermal-induced bending of four bilayer hydrogels clearly showed a bi-directional bending from initial negative bending to final positive bending, i.e. from -11.02 ° to -18.21 ° to 158.93 ° for GO3.R1000,

from -24.33 º to -59.15 º to 190.1 º for GO3.R2000, from -57.67 º to -124.82 º to 195.89 º GO3.R3000, and from -103.1 º to -197.1 º to 195.8 º for GO3.R4000, respectively. Clearly, the bending behavior of bilayer hydrogels also depends on centrifugation speed during the preparation process. GO3.R1000 and GO3.R2000 hydrogels prepared at 1000 and 2000 rpm exhibited minor bending toward the GO-rich side (negative angle of -11.02 ° and -24.33 º) in 25 ºC water and a large opposite bending toward the polyNIPAM layer (positive angle of 158.93 ° and 190.1 º) in 55 ºC water. However, the hydrogels fabricated at high speed centrifugation (3000 rpm and 4000 rpm) exhibited a different but interesting bending behavior. As a typical example shown in **Figure 3e**, GO3.R3000 hydrogel (prepared from 3.0 mg/ml GO and centrifugation speed of 3000 rpm) initially bent -50 º toward the GO-rich layer in 25 °C of water. Upon immersing the hydrogel into 55 °C of water for 25 s, the hydrogel continuously bent toward the same direction to achieve the max. negative bending angle of -120 º. After that, the hydrogel tended to bend backward the polyNIPAM layer in an opposite direction and finally achieved a final positive bending angle of ~200 ° at 90 s. This bidirectional bending behavior under one stimulus became more pronounced in the case of GO3.R4000. The continuous bending of GO3.R3000 and GO3.R4000 hydrogels toward GO-rich layer is a result from a cooperation between the initial negative bending in 25 °C of water and a fast shrinkage rate of GO-rich layer in 55 °C of water, followed by the backward bending induced by the larger shrinkage of polyNIPAM layer (**Figure S4**). So, a general trend of bending behavior is that high centrifugation speed leads to not only the higher bending angles, but also bi-directional bending in hot water. In all cases, the temperature-induced bending behavior of polyNIPAM/GO hydrogels is attributed to the fact that the increase of temperature leads to different shrinkage rates and volume changes between polyNIPAM layer and GO-rich layer, which provide the driving force to facilitate the bending behavior of bilayer hydrogels.

For a more practical purpose, we further tested the weight lifting capacity of polyNIPAM/GO bilayer hydrogel as driven by its bending actuation. Herein, we mounted copper wires of different weights (up to 1.5, 3.0, and 4.0 times in weight of the hydrogels, namely 1.5 m_0, 3.0 m_0, and 4.5 m_0) on GO1.R1000 and GO3.R3000 hydrogels. As shown in **Figure 4**, while both bilayer hydrogels carried extra weights, they still showed time-dependent thermal-induced bending. The bending kinetics trends were similar to that of the hydrogels without carrying any weight, but the hydrogels with carrying weights took longer time to achieve the same/similar bending angles than the hydrogel without carrying weight. Specifically, in **Figure 4a1-a2**, GO1.R1000 hydrogels with mounting of 1.5 m_0 and 3.0 m_0 copper wires took 26 s and 30 s to change their bending from -19.6 ° and -4.5 ° to -189.55 ° and -180 °, as compared to a control hydrogel that achieved the almost same bending angle for 22 s. With 4.5 m_0 carrying weight, GO1.R1000 hydrogel changed slowly its initial bending of -2.15 ° to -21.79 ° within 18 s, and further increase of time did not change the bending anymore. In the case of GO3.R3000 hydrogel (**Figure 4b1-b2**), the presence of copper weights significantly reduced the bi-directional bending degree. Within 70 s, maximal positive bending angle was decreased in an order of 200 °> 131.5 °> 104.8 °> 22.2 ° when carrying 0, 1.5 m_0, 3.0 m_0, and 4.5 m_0 weights. Clearly, the more carrying weight on hydrogels will result in a large decrease of bending angle and bending rate. Additionally, when the hydrogels were deformed by large external loading, the hydrogels showed a non-uniform bending, i.e. one free end of the gel was readily subject to bend, while another fixed end of the gel was almost resistance to bending. The non-uniform bending is likely caused by the non-uniform distribution of external loading exerted on different parts of the hydrogel strip, particularly at the fixed end of the hydrogel, the actual external loading is sum of the weights of both a copper and

the rest of the hydrogel. Consequently, such weight loading at the fixed end exceeds the lifting capacity of the hydrogel, thus leading to a very small or almost negligible bending of the hydrogel near the fixed end.

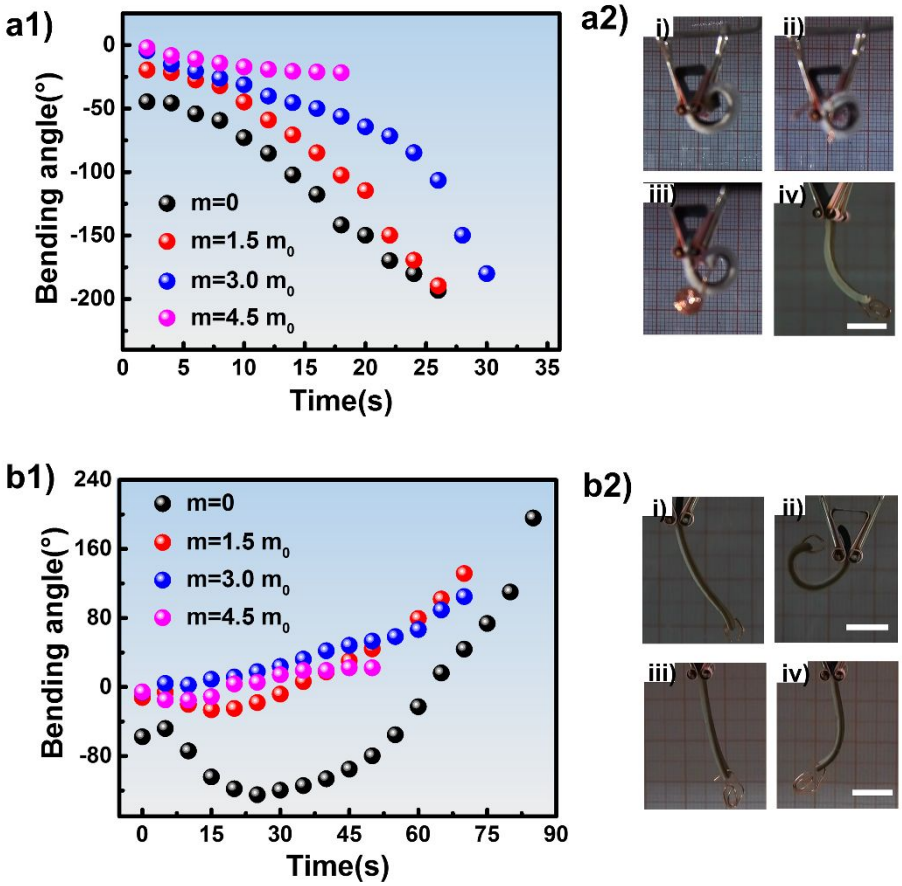

Figure 4. Bending kinetics of (a1) GO1.R1000 and b1) GO3.R3000 hydrogels carrying copper wire of different weight. (a2) Typical images of GO1.R1000 hydrogel carrying copper wires of (i) 0, (ii) 1.5 m_0, (iii) 3 m_0, and (iv) 4.5 m_0 during the bending process. (b2) Typical images of GO3.R3000 hydrogel carrying copper wires of (i, ii) 1.5 m_0 and (iii, iv) 4.5 m_0 during the bending process. Scale bar=1 cm.

As functional actuators, reversible and recoverable actuation is critical for practical applications.[46-47] Here, we further examined the multiple, reversible bending of bilayer hydrogels in response to temperature changes between 25 °C and 55 °C. As shown in **Figure 5a1**, the GO1.R1000 bilayer hydrogel initially bent -48.32 ° in 25 °C water. Upon immersing the hydrogel into 55 °C water for 22 s, the hydrogel rapidly curved to -189.55 ° along the same direction. After that, when the hydrogel was put back into 25 °C water for 30 min, it can completely recover its original bending of -48.32 °. In **Figure 5a2**, GO1.R1000 bilayer hydrogel demonstrated highly reversible and repeatable bending actuation between -48.32 ° in 25 °C water and -189.55 ° in 55 °C water up to 5 times. Unlike the single-directional bending of GO1.R1000 bilayer hydrogel, GO3.R3000 hydrogels exhibited reversible, bi-directional bending between -57.67 ° in 25 °C water, -120 ° and 195.89 ° in 55 °C water in five repeated cycles (**Figure 5b1-b2**). In both cases, no changes in the bending curvature, response time, and recovery time were observed within 5 cycles, confirming that polyNIPAM/GO bilayer hydrogels have reliable, reversible actuation.

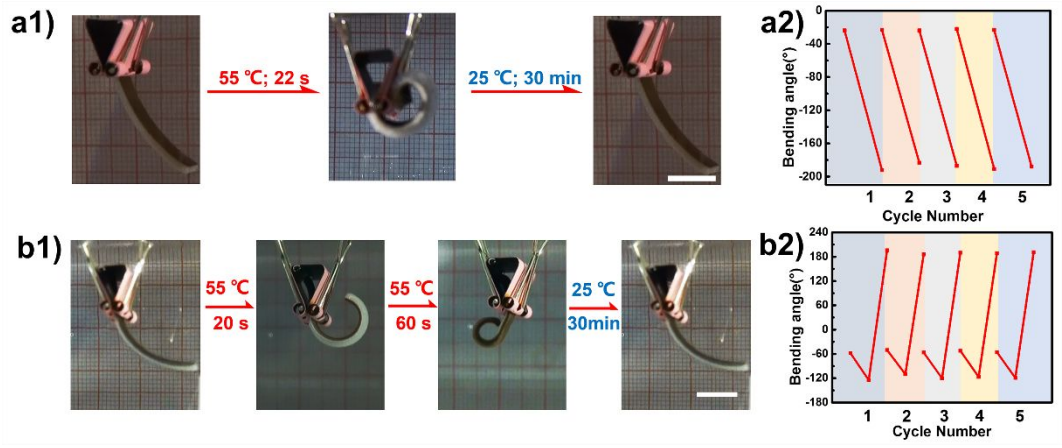

Figure 5. Multiple, reversible bending of (a1-a2) GO1.R1000 and (b1-b2) GO3.R3000 hydrogels in five repeated cycles between 25 °C and 55 °C water. Scale bar=1 cm.

The bending behavior of polyNIPAM/GO bilayer hydrogels in water at different temperature were also characterized to test the applicability of these hydrogels in a wide temperature range. Two exemplative hydrogels, i.e. GO1.R1000 and GO3.R3000, were used for this test. As shown in **Figure 6,** the hydrogels showed their corresponding bending behavior (unidirectional and bidirectional bending for GO1.R1000 and GO3.R3000, respectively) in the temperature range from 30 °C to 60 °C, and a trend that the bending angle increased as increasing temperature was observed. Even at 40 °C, GO1.R1000 hydrogel still exhibited a bending with angle of -144.7 °, and GO3.R3000 still showed negative bending and positive bending with angles of -65.5 ° and 104.4 °, respectively. The bending in a wide temperature range, particularly the bending at low temperature, would greatly expand the application of bilayer hydrogels.

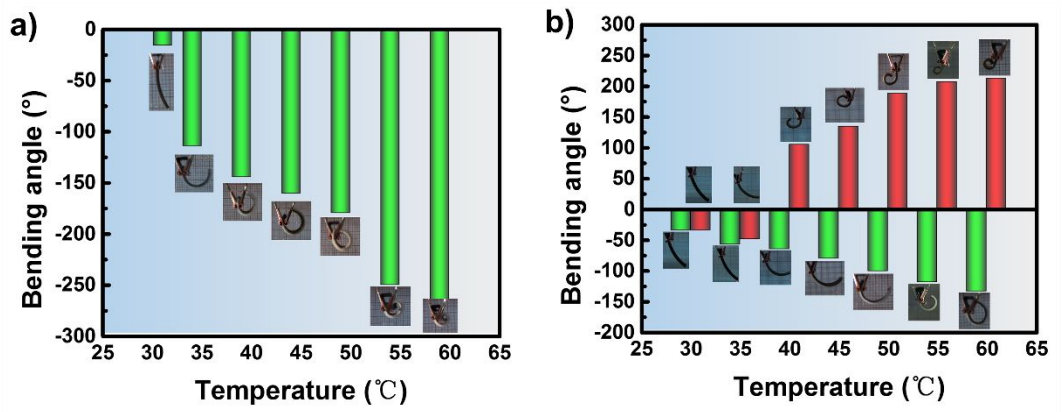

Figure 6. Bending angles of (a) GO1.R1000 and (b) GO3.R3000 hydrogels in the water at different temperatures.

The polyNIPAM/GO bilayers, particularly prepared at high concentration GO and high centrifugation speed, demonstrate their highly reversible, repeatable, and bi-directional bending capability. Based on this reversible, bi-directional bending behavior, we further designed two proof-of-concept hydrogel actuators, which act as a wiggler to mimic robot arms to push objects and a switch to turn on/off a light. As a first example in **Figure 7a-7b**, both GO1.R3000 and GO3.R3000 hydrogels can gradually bend towards GO-rich layer to push down aluminum (Al) piece from a platform in hot

water. But, GO3.R3000 hydrogel can also bend backward to push down Al piece from another direction, again demonstrating its bi-directional bending ability. The weight of Al piece was ~20-21 times of the hydrogel itself.

In the second example, GO3.R3000 hydrogel acts as an electrical switch to turn on/off lights in hot water. As shown in **Figure 7c-7d**, the hydrogel in hot water first bent to GO-rich layer to turn on the purple light in 20 s. Then, the backward bending occurred, during which the hydrogel first moved away from the electric circuit to turn off purple light, then continued to bend backward polyNIPAM layer, and finally established a new contact with the circuit and the green light was turned on at 80 s. Different from traditional hydrogel-based actuators that require different stimuli to realize bi-directional bending, our polyNIPAM/GO hydrogels provide a simple, reliable, bi-directional bending actuation under the same stimuli, without no necessary to change external stimuli.

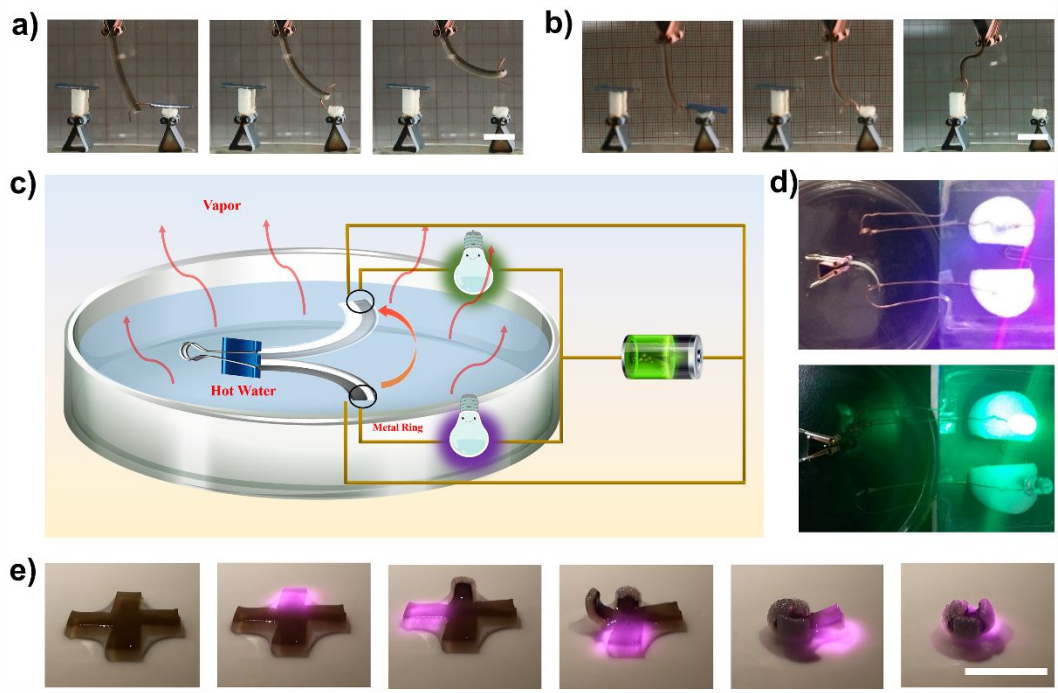

Figure 7. Conceptual actuator examples made of polyNIPAM/GO bilayer hydrogels. Representative images to demonstrate (a) GO1.R1000 and (b) GO3.R3000 hydrogels as wigglers for moving the aluminum sheet in 55 °C water along single-direction and bi-direction. (c) Schematic illustration and (d) experimental demonstration of GO3.R3000 hydrogel as an electric switch to turn on/off two lights in 55 °C water via bi-directional bending. (e) GO3.R3000 hydrogel shows a NIR responsive property (scale bar=1 cm).

Since GO sheets itself possess near-infrared (NIR) photothermal effect, polyNIPAM/GO bilayer hydrogels are expected to have NIR responsive properties. Here, we constructed a four-arm cross-shaped hydrogel to test its NIR responsive property. As shown in **Figure 7e**, when a laser with a wavelength of 808 nm and an intensity of 2.5 W/cm^2 was irradiated on one of a four-arm GO3.R3000 hydrogel, this arm was curled rapidly in 17 s and showed a pink color. Then, upon sequentially irradiating the other three arms of the hydrogel by the laser, all the arms were curled into a closed-flower-like shape, demonstrating the fast and strong NIR-responsive property of this hydrogel.

To prove that our gravity-induced fabrication method could be generally applicable to other polyNIPAM–nanoparticle hydrogels with a bilayer structure, we used SiO_2 nanoparticles to prepare polyNIPAM/SiO_2 bilayer hydrogels at different SiO_2 concentrations of 1.0 mg/ml and 3.0 mg/ml under centrifugation speed of 4000 rpm. All of these polyNIPAM/SiO_2 bilayer hydrogels exhibited similar temperature-induced bending behaviors, depending on SiO_2 concentration. As shown in **Figure 8a**, both polyNIPAM/SiO_2 bilayer hydrogels underwent a rapid single-direction bending from -5.04 ° to -149.68 ° for $SiO_2$3.R4000 toward the SiO_2-rich layer within 1 min. But, no bi-directional bending was observed (**Figure 8b**). We reasoned that high density of SiO_2 particles make them easily immigrate to one side of hydrogel under centrifugation and lead to a very thin SiO_2-rich layer, which can not sufficiently complete with the thermal-induced bending of the polyNIPAM layer.

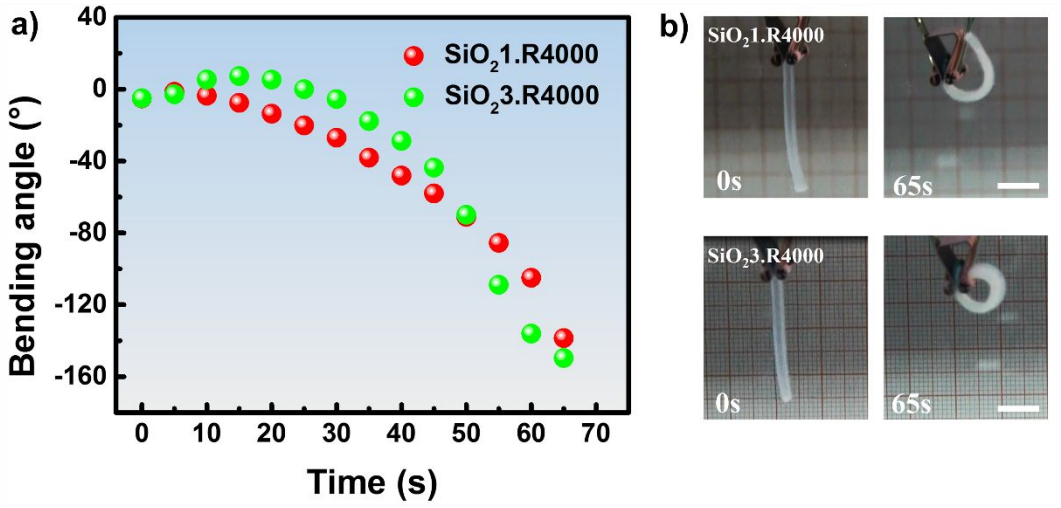

Figure 8. (a) Bending kinetics and (b) typical images of polyNIPAM/SiO_2 bilayer hydrogels actuating in 55 °C water (scale bar =1 cm).

CONCLUSIONS

In this work, we applied a new polymerization-centrifugation method to prepare dual-responsive polyNIPAM/GO bilayer hydrogels with a bilayer structure, consisting of a dark-brown, less-swelling dark-brown GO-rich layer and a transparent, highly swelling polyNIPAM layer. During the fabrication process, the high-gravity field was applied to drive GO nanoparticles move to one side, thus separating from the polyNIPAM layer and forming a bilayer structure. The working principle of this polyNIPAM/GO hydrogel actuation was mainly attributed to its asymmetric double-layer structure and distinct swelling behavior in each layer, which induced different bending directions in response to thermal and NIR stimulations, resulting in bi-directional bending behaviors. The bending actuation can be readily controlled by GO concentrations and centrifugation speeds. Within a minute, polyNIPAM/GO hydrogels exhibited not only fast bending actuation in hot water, but also reversible and repeatable bending responses by simply switching water of different temperatures. Based on rapid reversible bidirectional bending actions triggered by water temperatures, we further designed two different temperature-responsive hydrogel actuators, which realize an electric switch to turn on/off light and a wiggler to move an object, highlighting the advantages of the new system. Finally, we demonstrated the general applicability of our polymerization-centrifugation method by successfully

fabricating polyNIPAM/SiO_2 bilayer hydrogels with similar bending actuation behavior. Generally speaking, for hydrogel actuators requiring the operation in water, they could be used for soft robots in water, microgrippers for biological purposes, and smart valves for microfluidic applications. For the applications in hot water, they could be used as damage sensors. In addition, the NIR responsive properties also endow this hydrogel with some potentials as remotely controlled microgrippers. Our polyNIPAM/nanoparticle bilayer hydrogel systems, along with a general facile preparation method, possess great promising potentials for a variety of applications such as soft robots, artificial muscles, and intelligent human-machine interfacial materials.

Acknowledgement.

J.Y. thanks financial support from Natural Science Foundation of China (No.51673175), Natural Science Foundation of Zhejiang Province (LY16E030012), and Zhejiang Top Priority Discipline of Textile Science and Engineering (2015KF06). J.Z. thanks financial support from NSF grants (DMR-1607475 and CMMI-1825122). We also thank Hanqing Wang (Hangzhou No. 14 High School AP101, China) for her participation and assistance in this project during the summer.

REFERENCES

1 Yuk, H.; Lin, S.; Ma, C.; Takaffoli, M.; Fang, N. X.; Zhao, X., *Nat. Commun* 2017**, 8,** 14230.

2 Wang, J.; Wang, J.; Chen, Z.; Fang, S.; Zhu, Y.; Baughman, R. H.; Jiang, L., *Chem. Mater* 2017, **29 (22)**, 9793-9801.

3 Zhang, D.; Fu, Y.; Huang, L.; Zhang, Y.; Ren, B.; Zhong, M.; Yang, J.; Zheng, J., *J. Mater. Chem. B* 2018**, 6**, 950-960.

4 Xiao, S.; Zhang, M.; He, X.; Huang, L.; Zhang, Y.; Ren, B.; Zhong, M.; Chang, Y.; Yang, J.; Zheng, J., *ACS Appl. Mater. Interfaces* 2018**, 10 (25)**, 21642-21653.

5 Wu, Z. L.; Moshe, M.; Greener, J.; Therien-Aubin, H.; Nie, Z.; Sharon, E.; Kumacheva, E., *Nat. Commun.* 2013**, 4 (3)**, 1586.

6 L, W.; Y, J.; X, L.; W, L.; C, M.; J, Z.; Y, H.; CF, H.; T, C., *Chem. Commun* 2018**, 54**, 1229-1232.

7 Xiao, S.; Yang, Y.; Zhong, M.; Chen, H.; Zhang, Y.; Yang, J.; Zheng, J., *ACS Appl. Mater. Interfaces* 2017**, 9 (24)**, 20843–20851.

8 Peng, H. Y.; Wang, W.; Gao, F.; Lin, S.; Liu, L. Y.; Pu, X. Q.; Liu, Z.; Ju, X. J.; Xie, R.; and Chu, L. Y., J. Mater. Chem.C 2018, **6**, 11356

9 Zhang, F.; Fan, J.; Zhang, P.; Liu, M.; Meng, J.; Jiang, L.; Wang, S., *Npg Asia Mater.* 2017**, 9**, e380.

10 Zheng, S. Y.; Tian, Y.; Zhang, X. N.; Du, M.; Song, Y.; Wu, Z. L.; Zheng, Q., *Soft Matter* 2018**, 14**, 5888-5897.

11 Han, D. D.; Zhang, Y. L.; Ma, J. N.; Liu, Y. Q.; Han, B.; Sun, H. B., *Adv. Mater* 2016**, 28 (38)**, 8328-8343.

12 Zhang, H.; Mourran, A.; Mã¶Ller, M., *Nano Lett.* 2017**, 17 (3)**, 2010-2014.

13 Li, X.; Cai, X.; Gao, Y.; Serpe, M. J., *J. Mater. Chem. B* 2017**, 5**, 2804-2812.

14 Takahashi, R.; Sun, T. L.; Saruwatari, Y.; Kurokawa, T.; King, D. R.; Gong, J. P., *Adv. Mater.* 2018**, 30 (16)**, 1706885.

15 Yang, L.; Qi, K.; Chang, L.; Xu, A.; Hu, Y.; Zhai, H.; Lu, P., *J. Mater. Chem. B* 2018, **6**, 5031-5038.

16 Lin, Q. M.; Li, L. Y.; Tang, M.; Hou, X. S. and Ke, C. f., J. Mater. Chem.C 2018, **6**, 11956.

17 Zhang, X.; Pint, C. L.; Lee, M. H.; Schubert, B. E.; Jamshidi, A.; Takei, K.; Ko, H.; Gillies, A.; Bardhan, R.; Urban, J. J.; Wu, M.; Fearing, R.; Javey, A., *Nano Lett.* 2011**, 11 (8)**, 3239-3244.

18 Cheng, Y.; Ren, K.; Yang, D.; Wei, J., *Sensor. Actuat. B-Chem.* 2018**, 255**, 3117-3126.

19 Zhao, Q.; Liang, Y.; Ren, L.; Yu, Z.; Zhang, Z.; Qiu, F.; Ren, L., *J. Mater. Chem. B* 2018, **6**, 1260-1271.

20 Li, M.; Jiang, Z.; An, N.; Zhou, J., *Int. J. Mech. Sci.* 2018**, 140**, 271-278.

21 Shi, K.; Liu, Z.; Wei, Y. Y.; Wang, W.; Ju, X. J.; Xie, R.; Chu, L. Y., *ACS Appl. Mater. Interfaces* 2015**, 7 (49)**, 27289-27298.

22 Bassik, N.; Abebe, B. T.; Laflin, K. E.; Gracias, D. H., *Polymer* 2010**, 51 (26)**, 6093-6098.

23 Haque, M. A.; Kurokawa, T.; Gong, J. P., *Polymer* 2012**, 53 (9)**, 1805-1822.

24 Zheng, J.; Xiao, P.; Le, X.; Lu, W.; Théato, P.; Ma, C.; Du, B.; Zhang, J.; Huang, Y.; Chen, T., *J. Mater. Chem. C* 2018**, 6 (6)**, 1320-1327.

25 So, S.; Hayward, R. C., *ACS Appl. Mater. Interfaces* 2017**, 9 (18)**, 15785–15790.

26 Ma, C.; Lu, W.; Yang, X.; He, J.; Le, X.; Wang, L.; Zhang, J.; Serpe, M. J.; Huang, Y.; Chen, T., *Adv. Funct. Mater.* 2018**, 28 (7)**, 1704568.

27 Kim, J.; Kim, C.; Song, Y. S.; Jeong, S. G.; Kim, T. S.; Lee, C. S., *Chem. Eng. J.* 2017**, 321**, 384-393.

28 Cheng, Y.; Huang, C.; Yang, D.; Ren, K.; Wei, J., *J. Mater. Chem. B* 2018. **6 (48)**, 8170-8179

29 Zhao, L.; Huang, J.; Zhang, Y.; Wang, T.; Sun, W.; Tong, Z., *ACS Appl. Mater. Inter.* 2017**, 9 (13)**, 11866-11873.

30 Zheng, W. J.; An, N.; Yang, J. H.; Zhou, J.; Chen, Y. M., *ACS Appl. Mater. Interfaces* 2015**, 7 (3)**, 1758-1764.

31 Peng, X.; Liu, T.; Jiao, C.; Wu, Y.; Chen, N.; Wang, H.; Peng, X.; Liu, T.; Jiao, C.; Wu, Y., *J. Mater. Chem. B* 2017, **5***,* 7997-8003

32 Wang, E.; Desai, M. S.; Lee, S. W., Nano Lett. 2013, **13***,* 6, 2826-2830

33 Du, J.; Zhu, J.; Wu, R.; Xu, S.; Tan, Y.; Wang, J., *RSC Adv.* 2015**, 5 (74)**, 60152-60160.

34 Kim, D.; Lee, H. S.; Yoon, J., *Sci. Rep.* 2016**, 6**, 20921.

35 Yao, C.; Liu, Z.; Yang, C.; Wang, W.; Ju, X.-J.; Xie, R.; Chu, L.-Y., *Adv. Funct.Mater.* 2015**, 25 (20)***,* 2980-2991.

36 Teng, C.; Qiao, J.; Wang, J.; Jiang, L.; Zhu, Y., *ACS Nano* 2016**, 10 (1)***,* 413-420.

37 Fang, C.; Yang, K.; Zhou, Q.; Peng, K.; Yang, H., *RSC Adv.* 2018, **8 (61)***,* 35094-35101.

38 Tan, Y.; Xu, S.; Wu, R.; Du, J.; Sang, J.; Wang, J., *Appl. Clay Sci.* 2017**, 148**, 77-82.

39 Asoh, T. A.; Matsusaki, M.; Kaneko, T.; Akashi, M., *Adv. Mater.* 2010**, 20 (11)**, 2080-2083.

40 Tan, Y.; Wang, D.; Xu, H.; Yang, Y.; An, W.; Yu, L.; Xiao, Z.; Xu, S., *Macromol. Rapid Comm.* 2018**, 39 (8)**, 1700863 (1 of 6).

41 Wang, W.; Xiang, C.; Zhu, Q.; Zhong, W.; Li, M.; Yan, K.; Wang, D., *ACS Appl. Mater. Interfaces* 2018**, 10 (32)**, 27215-27223.

42 Tan, Y.; Wang, D.; Xu, H.; Yang, Y.; Wang, X.-L.; Tian, F.; Xu, P.; An, W.; Zhao, X.; Xu, S., *ACS Appl. Mater. Interfaces* 2018**, 10 (46)**, 40125-40131.

43 Yang, Y.; Tan, Y.; Wang, X.; An, W.; Xu, S.; Liao, W.; Wang, Y., *ACS Appl. Mater. Interfaces* 2018**, 10 (9)**, 7688-7692.

44 Tan, Y.; Wu, R.; Li, H.; Ren, W.; Xu, S.; Wang, J., *J. Mater. Chem. B* 2015**, 3 (21)**, 4426-4430.

45 Peng, X.; Jiao, C.; Zhao, Y.; Chen, N.; Wu, Y.; Liu, T.; Wang, H., *ACS Appl. Nano Mater.* 2018**, 1 (4)**, 1522-1530.

46 Amjadi, M.; Sitti, M., *Adv. Sci.* 2018*,* **5**, 1800239.

47 Amjadi, M.; Sitti, M., *Acs Nano* 2016**, 10**, 10202−10210.